UvA-DARE (Digital Academic Repository)

X-Ray Emission and Absorption Features during an Energetic Thermonuclear X-Ray Burst from IGR J17062-6143

Degenaar, N.; Miller, J.M.; Wijnands, R.; Altamirano, D.; Fabian, A.C.

Link to publication

X-RAY EMISSION AND ABSORPTION FEATURES DURING AN ENERGETIC THERMONUCLEAR X-RAY BURST FROM IGR J17062−6143

N. Degenaar[1,4], J. M. Miller[1], R. Wijnands[2], D. Altamirano[2], and A. C. Fabian[3]

[1] Department of Astronomy, University of Michigan, 500 Church Street, Ann Arbor, MI 48109, USA; degenaar@umich.edu
[2] Astronomical Institute "Anton Pannekoek," University of Amsterdam, Postbus 94249, 1090 GE Amsterdam, The Netherlands
[3] Institute of Astronomy, University of Cambridge, Madingley Road, Cambridge CB3 OHA, UK

ABSTRACT

Type-I X-ray bursts are thermonuclear explosions occurring in the surface layers of accreting neutron stars. These events are powerful probes of the physics of neutron stars and their surrounding accretion flow. We analyze a very energetic type-I X-ray burst from the neutron star low-mass X-ray binary IGR J17062−6143 that was detected with *Swift* on 2012 June 25. The light curve of the $\simeq$18 minute long X-ray burst tail shows an episode of $\simeq$10 minutes during which the intensity is strongly fluctuating by a factor of $\simeq$3 above and below the underlying decay trend on a timescale of seconds. The X-ray spectrum reveals a highly significant emission line around $\simeq$1 keV, which can be interpreted as an Fe-L shell line caused by the irradiation of cold gas. We also detect significant absorption lines and edges in the Fe-K band, which are strongly suggestive of the presence of hot, highly ionized gas along the line of sight. None of these features are present in the persistent X-ray spectrum of the source. The timescale of the strong intensity variations, the velocity width of the Fe-L emission line (assuming Keplerian motion), and photoionization modeling of the Fe-K absorption features each independently point to gas at a radius of $\simeq$10^3 km as the source of these features. The unusual X-ray light curve and spectral properties could have plausibly been caused by a disruption of the accretion disk due to the super-Eddington fluxes reached during the X-ray burst.

Key words: accretion, accretion disks – stars: neutron – X-rays: binaries – X-rays: individual (IGR J17062−6143)

Online-only material: color figures

1. INTRODUCTION

Type-I X-ray bursts are intense flashes of X-ray emission that have a duration of seconds to hours. These events are caused by unstable thermonuclear burning, which transforms the hydrogen and/or helium that is accreted onto the surface of a neutron star into heavier elements (for reviews, see Lewin et al. 1995; Strohmayer & Bildsten 2006; Schatz & Rehm 2006). The light curves of X-ray bursts are characterized by a fast rise that is caused by burning of the fuel layer, followed by a slower decay phase that represents cooling of the burning ashes. Their X-ray spectra can be modeled by blackbody emission that peaks at a temperature of $\simeq$2–3 keV and cools to $\simeq$1 keV in the tail of the X-ray burst.

The peak radiation of X-ray bursts can exceed the Eddington limit, which causes the photosphere to expand. This can be observed as an increase in blackbody emission radius (typically by a factor of a few) that is accompanied by a decrease in effective temperature while maintaining an approximately constant flux. On rare occasions, X-ray bursts have been observed to be so powerful that the emission radius increased by a factor of $\simeq$100. This is denoted as superexpansion (in 't Zand & Weinberg 2010).

X-ray bursts are a unique signature of neutron star low-mass X-ray binaries (LMXBs). In LMXBs, a Roche-lobe overflowing late-type companion star feeds matter to the compact object via an accretion disk. There is a delicate connection between the properties of X-ray bursts and that of the accretion flow. For example, the rate at which mass is accreted onto the neutron star determines the duration and recurrence time of X-ray bursts (e.g., Fujimoto et al. 1981; Bildsten 1998; Peng et al. 2007), and

the accretion geometry can strongly influence their observable properties (e.g., Cavecchi et al. 2011; Linares et al. 2012; in 't Zand et al. 2012). On the other hand, there are several lines of evidence suggesting that powerful X-ray bursts can affect the accretion flow (Yu et al. 1999; Strohmayer & Brown 2002; Ballantyne & Strohmayer 2004; Kuulkers et al. 2009; Chen et al. 2011; in 't Zand et al. 2011; Altamirano et al. 2012).

IGR J17062−6143 is an X-ray source that was discovered with *INTEGRAL* in 2006 (Churazov et al. 2007). It has been active ever since, displaying a 2–10 keV luminosity of $L_X \simeq (1–5) \times 10^{35}(D/5.0\,\mathrm{kpc})^2\,\mathrm{erg\,s^{-1}}$ (Ricci et al. 2008; Remillard & Levine 2008; Degenaar et al. 2012). IGR J17062−6143 remained unclassified until *Swift*'s Burst Alert Telescope (BAT; Barthelmy et al. 2005) detected an X-ray burst on 2012 June 25 (Barthelmy et al. 2012), which identified the source as an accreting neutron star LMXB (Degenaar et al. 2012). In this Letter we report on unusual features present in the light curve and spectrum of this X-ray burst.

2. OBSERVATIONS, DATA ANALYSIS, AND RESULTS

The BAT triggered on IGR J17062−6143 on UT 2012 June 25 at 22:42 (Barthelmy et al. 2012). The X-Ray Telescope (XRT; Burrows et al. 2005) began to observe the source in the windowed timing (WT) mode $\simeq$157 s later, for a total exposure time of 927 s (ObsID 525148000). We reduced and analyzed the *Swift* data using the HEASOFT software package (ver. 6.11).

The BAT and XRT data were processed using the BATGRBPRODUCT and XRTPIPELINE tools, respectively. We extracted BAT light curves and spectra with BATBINEVT, and used XSELECT for the XRT data. To avoid pile-up, we used an annular extraction region with an inner (outer) radius of 2 (40) pixels when the XRT count rate exceeded 200 counts s^{-1}, and

---

radii of 1 (40) pixels when the count rate was 100–200 counts s^{-1} (Romano et al. 2006). For lower intensities we used a circular region with a radius of 40 pixels.

The XRT spectral data were grouped into bins with a minimum of 20 photons and fitted between 0.5 and 10 keV using XSPEC (ver. 12.7; Arnaud 1996). The BAT spectrum was fitted between 15 and 40 keV. We accounted for interstellar absorption by using the TBABS model (Wilms et al. 2000). The quoted errors represent 1σ confidence intervals.

2.1. The BAT X-Ray Burst Peak

The source is detected with the BAT for $\simeq 160$ s, peaking at $t \simeq 80$ s after the trigger. The average spectrum, extracted from $t = 0$–160 s, can be described by a blackbody model with a temperature of $kT_{bb} = 2.6 \pm 0.3$ keV and an emitting radius of $R_{bb} = 4.9^{+2.8}_{-1.7}$ km (for an assumed distance of 5.0 kpc; see below). By extrapolating the fit to the 0.01–100 keV energy range, we estimate an average bolometric flux of $F_{bol} = 4.8^{+2.8}_{-1.6} \times 10^{-8}$ erg cm^{-2} s^{-1}. This gives a fluence for the X-ray burst peak of $f_{BAT} \simeq 7.7 \times 10^{-6}$ erg cm^{-2}.

The peak count rate observed with the BAT is a factor of $\simeq 2.6$ higher than the average intensity in the 160 s interval, which suggests that the bolometric flux peaked at $\simeq 1.25 \times 10^{-7}$ erg cm^{-2} s^{-1}. Equating this to the empirical Eddington limit of X-ray bursts (3.8×10^{38} erg s^{-1}; Kuulkers et al. 2003) places the source at a distance of $D \simeq 5.0$ kpc (see also Degenaar et al. 2012).

2.2. Light Curve of the X-Ray Burst Tail

The XRT light curve shows a decrease in intensity from $\simeq 300$ to $\simeq 10$ counts s^{-1} (Figure 1). The overall decay is best described by a simple linear function with a slope of -0.32 counts s^{-2} and a normalization of 296.5 ± 0.9 counts s^{-1} at the start of the XRT observation. At $\simeq 390$ s after the BAT trigger, the source intensity starts to strongly fluctuate by as much as a factor of $\simeq 3$ above and below the underlying decay trend. The variations have a typical duration of seconds, and continue for $\simeq 590$ s. Timing analysis did not reveal periodicities (see also Degenaar et al. 2012).

Investigation of the ratio of the counts in the 2.5–10 keV and 0.3–2.5 keV energy bands shows that the hardness decreased over time (i.e., the spectrum became softer; Figure 1). The hardness ratio drops at the start of the fluctuation phase, but after that there is no apparent correlation between the intensity and the spectral hardness until $\simeq 250$ s before the variations disappear. In that final part of the fluctuation phase the hardness ratio is positively correlated with the intensity (Figure 1). The initial energy independence suggests that the plasma causing the fluctuations is in thermal balance with the radiation field, which appears to break down shortly before the variations disappear.

2.3. Spectrum of the X-Ray Burst Tail

We investigate the average XRT spectrum to obtain a global characterization of the X-ray burst. A single absorbed blackbody does not provide an adequate description of the XRT data ($\chi^2_{\nu} > 2$ for 744 dof). The fit can be improved by adding a power-law component ($\chi^2_{\nu} = 1.91$ for 742 dof), or a second blackbody ($\chi^2_{\nu} = 1.72$ for 742 dof), although neither provide a formally acceptable fit. Any reasonable combination of continuum components leaves a strong emission line at $\simeq 1$ keV.
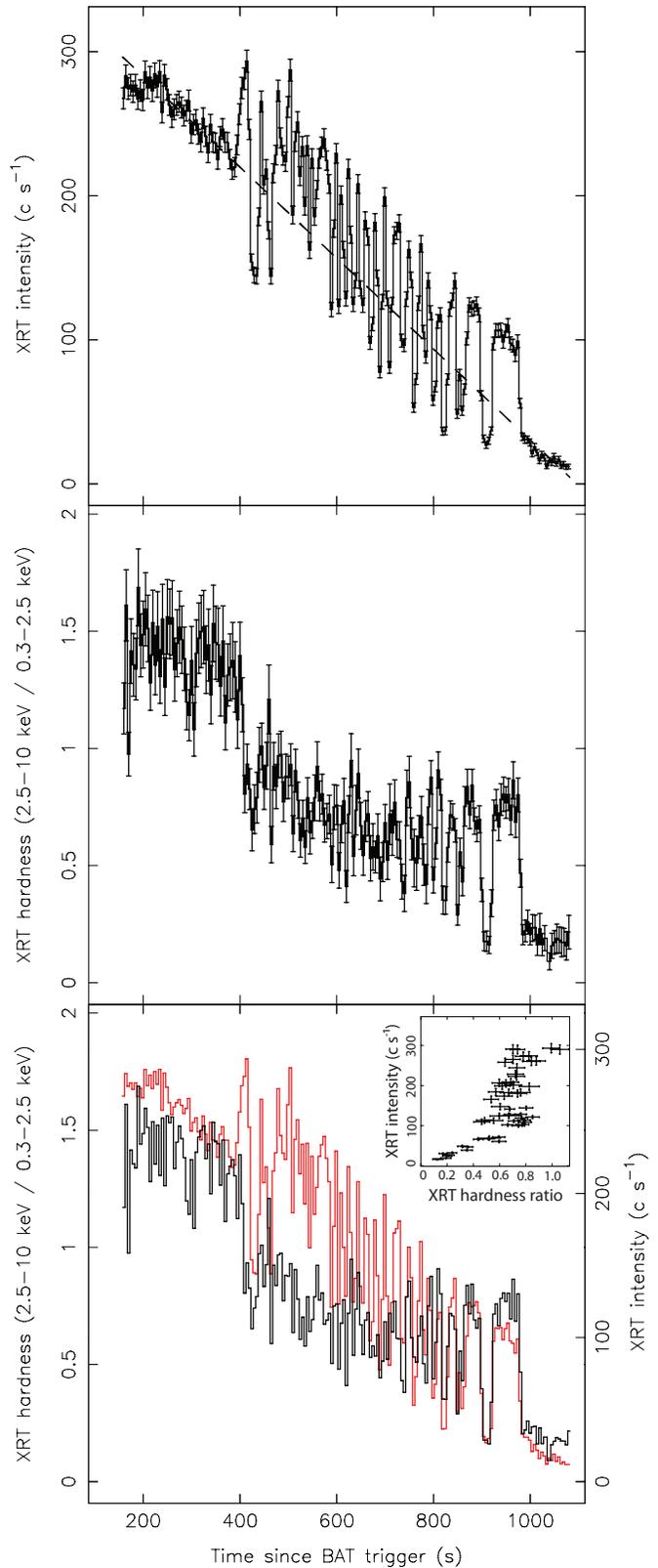
Figure 1. *Swift*/XRT data of the X-ray burst tail at 5 s resolution. Top: count rate light curve (0.3–10 keV). The dashed line indicates a fit to a linear decay with a slope of -0.32 counts s^{-2}. Middle: ratio of counts in the 2.5–10 keV and 0.3–2.5 keV energy bands. Bottom: combined plot of the hardness ratio (black) and count rate light curve (red). Error bars were omitted for clarity. The inset displays the intensity vs. the hardness during the fluctuating part of the light curve ($\simeq 390$–980 s after the BAT trigger).

(A color version of this figure is available in the online journal.)

Table 1
Spectral Parameters for the X-Ray Burst Tail

Model Component	Parameter (unit)	Average	Before Fluctuations	Fluctuations	After Fluctuations
TBABS	$N_H (\times 10^{21} \, \text{cm}^{-2})$	1.63 ± 0.04	...	1.43 ± 0.14	...
BBODYRAD1	kT_{bb} (keV)	1.787 ± 0.005	2.082 ± 0.025	1.584 ± 0.011	1.423 ± 0.013
BBODYRAD1	R_{bb} (D/5.0 kpc km)	5.49 ± 0.01	6.22 ± 0.03	5.43 ± 0.02	1.53 ± 0.16
BBODYRAD2	kT_{bb} (keV)	0.258 ± 0.001	0.260 ± 0.008	0.256 ± 0.006	0.213 ± 0.008
BBODYRAD2	R_{bb} (D/5.0 kpc km)	83.56 ± 0.01	81.33 ± 0.18	86.60 ± 0.14	68.18 ± 0.20
GAUSSIAN1: Emission	E_1 (keV)	1.018 ± 0.004	1.017 ± 0.006	1.029 ± 0.006	1.000 ± 0.010
GAUSSIAN1: Emission	σ ($\times 10^{-2}$ keV)	6.73 ± 0.44	7.76 ± 0.84	7.52 ± 1.28	7.16 ± 1.97
GAUSSIAN1: Emission	Norm. ($\times 10^{-2}$ photons cm^{-2} s^{-1})	8.22 ± 0.30	15.2 ± 1.25	6.69 ± 0.68	4.64 ± 0.73
GAUSSIAN2: Abs. Fe XXV	E_1 (keV)	7.73 ± 0.03	...	7.73 fixed	...
GAUSSIAN2: Abs. Fe XXV	σ (keV)	0 fixed	...	0 fixed	...
GAUSSIAN2: Abs. Fe XXV	Norm. ($\times 10^{-3}$ photons cm^{-2} s^{-1})	5.9 ± 1.2	...	4.3 ± 0.8	...
GAUSSIAN3: Abs. Fe XXVI	E_1 (keV)	8.10 ± 0.03	...	8.10 fixed	...
GAUSSIAN3: Abs. Fe XXVI	σ (keV)	0 fixed	...	0 fixed	...
GAUSSIAN3: Abs. Fe XXVI	Norm. ($\times 10^{-3}$ photons cm^{-2} s^{-1})	6.6 ± 1.2	...	4.4 ± 0.9	...
EDGE: Fe XXV	E_c (keV)	8.8 fixed	...	8.8 fixed	...
EDGE: Fe XXV	τ	0.50 ± 0.09	...	0.40 ± 0.12	...
EDGE: Fe XXVI	E_c (keV)	9.3 fix	...	...	...
EDGE: Fe XXVI	τ	<0.07	...	...	...
...	χ_ν^2/dof	1.07/733	...	1.17/1427	...

Notes. Quoted errors represent a 1σ confidence level. The spectra of the intervals before, during, and after the fluctuation phase were fitted simultaneously with N_H tied.

Adding a Gaussian line to a continuum consisting of two black bodies improves the fit significantly ($\chi_\nu^2 = 1.18$ for 739 dof). The line has a centroid energy of $E_1 = 1.018 \pm 0.004$ keV, a width of $\sigma = (6.73 \pm 0.44) \times 10^{-2}$ keV, and a normalization of $(8.22 \pm 0.30) \times 10^{-2}$ photons cm^{-2} s^{-1} (Table 1). These line properties correspond to an equivalent width of 105 ± 3 eV. Dividing the normalization by its error indicates that the line is highly significant at the 27σ level of confidence. Assuming that abundances are not unusual and velocity shifts are modest, the 1 keV feature is most likely an Fe-L shell line or possibly a combination of a few such lines from a range of charge states (Ne X is also in this range). The line is detected at all intervals during the burst (Section 2.3.1), while it is not present in the persistent X-ray spectrum of the source (Figure 2).

In addition to the 1 keV emission feature, there are structures visible in the Fe-K band between $\simeq 7$ and 10 keV (Figure 3). Absorption lines consistent with Fe XXV Heβ (7.88 keV), Fe XXVI Lyβ (8.25 keV), and K edges associated with Fe XXV (8.8 keV) and Fe XXVI (9.3 keV) are evident. Adding two edges and two Gaussian absorption lines further improves the spectral fit ($\chi_\nu^2 = 1.07$ for 733 dof). The normalizations of the Gaussians suggest that the absorption lines are significant at the 5σ–6σ level of confidence. The inclusion of an edge at 8.8 keV is similarly significant (5.6σ), although the edge at 9.3 keV is statistically not required. The presence of these Fe-K band features is strongly suggestive of highly ionized absorption along the line of sight.

The best-fit results for the average X-ray burst spectrum are listed in Table 1. The temperature and emitting radius of the first blackbody component ($kT_{bb} \simeq 1.8$ keV and $R_{bb} \simeq 5$ km) are typical for the tails of X-ray bursts. The second blackbody is cooler and more extended ($kT_{bb} \simeq 0.3$ keV and $R_{bb} \simeq 80$ km), and could possibly arise from the (inner) accretion disk. The first blackbody (representing the X-ray burst emission) accounts for $\simeq 90\%$ of the total unabsorbed 0.5–10 keV flux of $F_X = (1.16 \pm 0.01) \times 10^{-8}$ erg cm^{-2} s^{-1}. By extrapolating this component to the 0.01–100 keV energy range while setting

the normalization of all others to zero, we estimate a thermal bolometric flux of $F_{bol} = (1.28 \pm 0.02) \times 10^{-8}$ erg cm^{-2} s^{-1} for the X-ray burst tail.

2.3.1. Time-resolved Spectroscopy

We extracted separate spectra from intervals before, during, and after the fluctuation phase by selecting data from $t =$ 157–390, 391–980, and 981–1084 s since the BAT trigger, respectively. We fit the three spectra simultaneously using the best-fit model found from analyzing the average X-ray burst spectrum. The results are summarized in Table 1.

The first blackbody displays the characteristic cooling seen during X-ray burst tails: the temperature decreases from $kT_{bb} = 2.08 \pm 0.02$ to 1.42 ± 0.13 keV (Table 1). The fractional contribution of this model component to the total 0.5–10 keV unabsorbed flux decreases from $\simeq 99\%$ to $\simeq 68\%$. The 1 keV emission feature is detected during the entire X-ray burst with a significance of 12.2σ, 9.8σ, and 6.4σ for the intervals before, during, and after the fluctuation phase, respectively (Figure 2). The line flux decreases over time, but the energy and width do not change significantly (Table 1). The Fe-K band absorption lines are present during the fluctuation phase (4σ–5σ level), as is the edge at 8.8 keV (3σ). These features are not significantly detected before and after this interval, which is plausibly due to the lower statistics.

2.3.2. X-Ray Spectra of the Peaks and Dips

We extracted separate spectra for the peaks and the dips of the fluctuation phase by separating the points lying above and below the linear decay fit (dashed line in Figure 1). We fit the two spectra simultaneously using the best-fit model found from analyzing the average X-ray burst spectrum.

The Fe-K band absorption features are not significantly detected in the separate spectra, but the Fe-L emission remains highly significant at the 8σ–10σ level. We find that the line is slightly shifted toward the red for the dip spectrum when
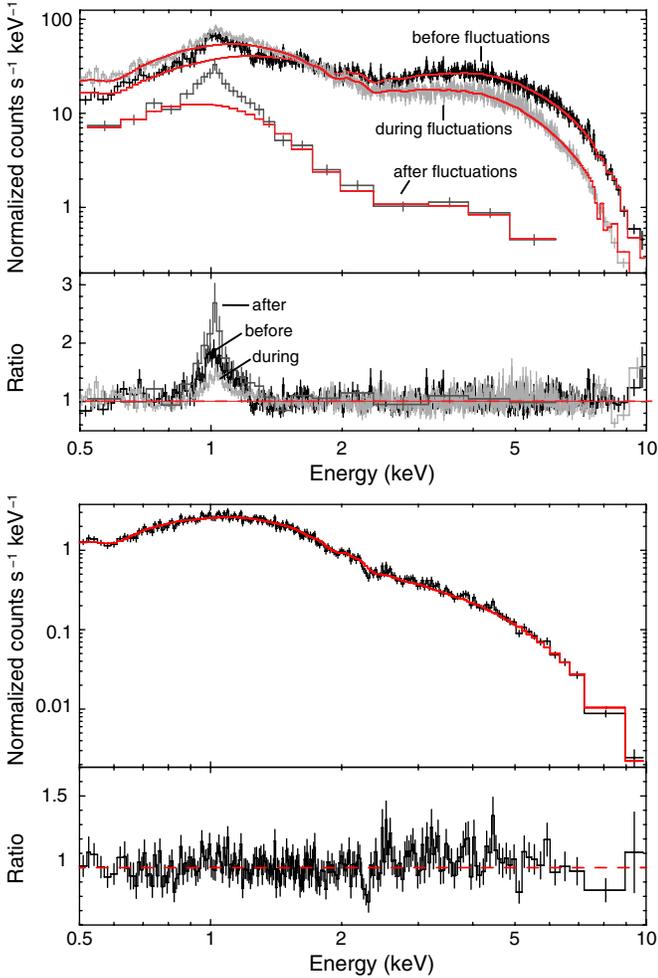
Figure 2. *Swift*/XRT WT mode spectra of IGR J17062−6143 (top panels) and data to model ratios (bottom panels). The solid red lines indicate the fitted continuum models. The spectra were rebinned for representation purposes. Left: X-ray burst spectra before (black), during (light gray), and after (dark gray) the fluctuation phase, with the normalization of the Fe-L emission line set to zero. Right: average spectrum of the persistent X-ray emission as observed in 2008 May (Ricci et al. 2008; Degenaar et al. 2012).

(A color version of this figure is available in the online journal.)

compared to that of the peaks; $E_{l,dips} = 1.028 \pm 0.007$ and $E_{l,peaks} = 1.050 \pm 0.010$ keV. The width of the line is similar in the two spectra ($\sigma_{peaks} = 0.109 \pm 0.016$ keV and $\sigma_{dips} = 0.090 \pm 0.014$ keV), but the normalization is larger for the dips; $(10.6 \pm 1.0) \times 10^{-2}$ photons cm^{-2} s^{-1} compared to $(7.5 \pm 1.1) \times 10^{-2}$ photons cm^{-2} s^{-1} for the peaks. These differences may indicate that emission from a lower charge state, at larger radius, is relatively more important during the dips.

2.4. Photoionization Modeling

In order to provide a physical characterization of the highly ionized absorption spectrum, we briefly explored fits using different grids of photoionization models created with XSTAR (Kallman & Bautista 2001). The fact that we observe He-like and H-like absorption lines requires a high ionization parameter. The prominence of putative β-lines combined with weakness (absence) of α-lines implies a high column density and saturation.

The best example of dense absorption in the Fe-K band was observed in the black hole LMXB GRO J1655−40 (Miller
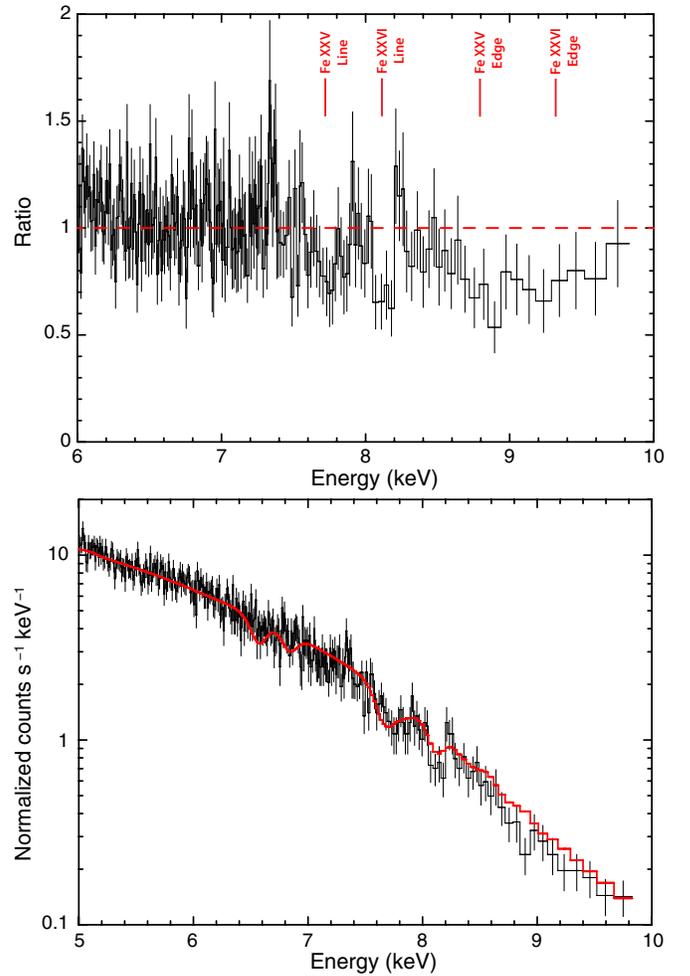
Figure 3. High-energy part of the average *Swift*/XRT spectrum of the X-ray burst tail. Top: ratio of the data and the continuum model. Bottom: spectral data compared to an XSTAR model developed for GRO J1655−40 (solid red line; from Miller et al. 2008).

(A color version of this figure is available in the online journal.)

et al. 2006, 2008). The continuum seen in the *Chandra*/HETGS spectrum of that source (an even mixture of a $kT = 1.35$ keV disk and a $\Gamma = 3.5$ power law at an overall luminosity of $L_X \simeq 5 \times 10^{37}$ erg s^{-1}) is comparable to the time-averaged spectrum of the X-ray burst in IGR J17062−6143 (which can be roughly described by a $kT_{bb} \simeq 1.8$ keV blackbody and a $\Gamma \simeq 3.7$ power law, yielding $L_X \simeq 3.5 \times 10^{37}$ erg s^{-1}). The grid used in models 1C and 3C for GRO J1655−40 in Miller et al. (2008) gives a good fit to the Fe-K absorption spectrum in the X-ray burst of IGR J17062−6143 (Figure 3). From this fit we measure a column density of $N = (5.0 \pm 1.0) \times 10^{23}$ cm^{-2}, an ionization parameter of $\log(\xi) = 5.0 \pm 0.5$, and a red shift of $(6 \pm 1) \times 10^3$ km s^{-1}.

Given that $\xi = L/nr^2$ erg cm s^{-1}, we can estimate the distance of the scattering medium from the neutron star. If we assume an X-ray burst luminosity of $L = 10^{38}$ erg s^{-1} and that the column density is related to the matter density via $N = nr$, then a radius of $r \simeq (0.3–2.5) \times 10^3$ km is implied by our fit.

2.5. Energetics of the X-Ray Burst

Extrapolating the linear fit to the X-ray burst light curve (Section 2.2) down to the intensity of the persistent emission measured in 2008 ($\simeq 5$ counts s^{-1}) suggests that the event had

a total duration of $\simeq 1100$ s ($\simeq 18$ minutes; see also Degenaar et al. 2012). This indicates that the XRT observation covered almost the entire burst tail and provides a good measure of the radiated energy output.

We integrate the decay fit over the full XRT observation, and apply the count rate to (thermal) bolometric flux conversion factor inferred from time-resolved spectroscopy of the X-ray burst tail (Section 2.3.1). This yields a fluence of $f_{\mathrm{XRT}} \simeq 1.1 \times 10^{-5}$ erg cm^{-2}. Combined with the X-ray burst peak (Section 2.1), we obtain a total fluence of $f_{\mathrm{b}} \simeq 1.9 \times 10^{-5}$ erg cm^{-2}. For a source distance of $D = 5.0$ kpc, the total radiated energy is $E_{\mathrm{b}} \simeq 6 \times 10^{40}$ erg.

3. DISCUSSION

We investigated an X-ray burst detected from the neutron star LMXB IGR J17062−6143 with *Swift* on 2012 June 25. The duration ($\simeq 18$ minutes) and total radiated energy output ($E_{\mathrm{b}} \simeq 5 \times 10^{40}$ erg) classify it as a rare, energetic intermediate-duration X-ray burst (e.g., in 't Zand et al. 2005; Degenaar et al. 2010, 2011). These represent only a few percent of the total number of observed X-ray bursts (Falanga et al. 2008; Keek et al. 2010).

During an interval of $\simeq 390$–980 s after the X-ray burst peak, the intensity strongly fluctuated by a factor of $\simeq 3$ above and below the underlying decay trend, on a timescale of seconds. Out of the thousands of X-ray bursts that have been observed from $\simeq 100$ LMXBs (e.g., Galloway et al. 2008; Keek et al. 2010), similar variability has only been reported for five X-ray bursts from four different sources (van Paradijs et al. 1990; Strohmayer & Brown 2002; Molkov et al. 2005; in 't Zand et al. 2005, 2011). Comparison of their properties suggests that superexpansion is a possible requisite for the occurrence of fluctuations (in 't Zand et al. 2011). The broad BAT peak, the long XRT tail, and the high radiative energy output all make it plausible that the X-ray burst of IGR J17062−6143 was powerful enough to drive a superexpansion phase.

Time-resolved (continuum) spectroscopy of superexpansion bursts has shown that the photosphere can be driven out to radial distances of $\simeq 10^3$ km (e.g., in 't Zand & Weinberg 2010; in 't Zand et al. 2011). It has been proposed that superexpansion can disrupt the accretion disk, and that the observed intensity fluctuations are caused by swept-up clouds of plasma or puffed-up structures in the disk (in 't Zand et al. 2011). If we assume that this plasma moves in Keplerian orbits, then the timescale of the fluctuations seen for IGR J17062−6143 ($P \simeq 1$–10 s) implies a radial distance of $r = (P^2 GM/4\pi^2)^{1/3} \simeq (2$–$8) \times 10^3$ km (for $M = 1.4\,M_\odot$).

Spectral analysis of the X-ray burst tail revealed a highly significant emission line around $\simeq 1$ keV in the Fe-L band. This emission feature can be explained through the irradiation of relatively cold gas. If we assume that the line is dynamically broadened, we can estimate the radial distance of this material. The measured width of $\sigma = 6.73 \times 10^{-2}$ keV gives a FWHM of 0.158 keV. Dividing this by the line energy ($E_1 = 1.018$ keV) suggests a velocity of $v \simeq 0.16c$. Assuming that the material is in a Keplerian orbit would imply a radial distance of $r = GM/v^2 \simeq 8 \times 10^2$ km from the neutron star.

We also found significant absorption features in the Fe-K band; absorption lines at $\simeq 7.73$ and $\simeq 8.10$ keV, which likely represent Fe xxv Heβ (7.88 keV) and Fe xxvi Lyβ (8.25 keV), as well as K edges consistent with Fe xxv (8.8 keV) and Fe xxvi (9.3 keV). By fitting the absorption features with photoionization models we inferred a radial distance of

$r \simeq (0.3$–$2.5) \times 10^3$ km for the hot, ionized material (Section 2.4). The spectral fits suggest a modest redshift for the putative absorption lines of $\simeq 6 \times 10^3$ km s^{-1}. This could be in line with the radial distance, since the free-fall velocity at 10^3 km is on the order of $\simeq 10^4$ km s^{-1}. However, velocity shifts of $\simeq 20$–50 eV might also arise through a drift in the gain calibration of the CCD (A. Beardmore 2012, private communication).

Disruption of the accretion disk by super-Eddington fluxes can plausibly have given rise to the Fe-L and Fe-K band atomic features (e.g., Day & Done 1991; Ballantyne & Strohmayer 2004; Ballantyne & Everett 2005). The radial distance found from fitting the Fe-K band absorption features is broadly consistent with that implied by spectral fits to the Fe-L emission line. The latter could arise due to the illumination of cold blobs of gas, which may be pressure-confined within hotter gas that is seen in absorption. Both components of the gas must have rotational support and be executing nearly Keplerian orbits, since the fallback time from a radial distance of $r \simeq 10^3$ km is $\simeq 0.1$ s. The distance and velocity estimates arising from our analysis of these atomic features are similar to those inferred from time-resolved continuum spectroscopy of superexpansion X-ray bursts (in 't Zand & Weinberg 2010).

We note that Fe-K emission lines and absorption edges have been reported for a handful of X-ray bursts (van Paradijs et al. 1990; Strohmayer & Brown 2002; in 't Zand & Weinberg 2010). However, to our knowledge it is the first time that such features are unambiguously detected during an X-ray burst at CCD resolution. Fe-L emission has not been seen before; the far majority of X-ray bursts have been observed with instruments that did not have coverage below 2 keV (e.g., *BeppoSAX*/WFC, *RXTE*, and *INTEGRAL*).

The timescale of the strong variations in the X-ray burst light curve implies a similar radial distance as inferred from the spectral absorption and emission features. It is therefore likely that all are caused by the same material and mechanism. We conclude that there are three independent lines of evidence that suggest that the energetic X-ray burst from IGR J17062−6143 involved a superexpansion phase that may have disrupted the (inner) accretion disk out to $\simeq 10^3$ km ($\simeq 50R_{\mathrm{g}}$ with $R_{\mathrm{g}} = RM/c^2$ the neutron star gravitational radius).

REFERENCES

Altamirano, D., Keek, L., Cumming, A., et al. 2012, MNRAS, 426, 927
Arnaud, K. A. 1996, in ASP Conf. Ser. 101, Astronomical Data Analysis Software and Systems V, ed. G. H. Jacoby & J. Barnes (San Francisco, CA: ASP), 17
Ballantyne, D. R., & Everett, J. E. 2005, ApJ, 626, 364
Ballantyne, D. R., & Strohmayer, T. E. 2004, ApJL, 602, L105
Barthelmy, S. D., Barbier, L. M., Cummings, J. R., et al. 2005, SSRv, 120, 143
Barthelmy, S. D., Baumgartner, W. H., Burrows, D. N., et al. 2012, GCN, 13386
Bildsten, L. 1998, in NATO ASIC Proc. 515, The Many Faces of Neutron Stars, ed. R. Buccheri, J. van Paradijs, & A. Alpar (Dordrecht: Kluwer), 419
Burrows, D. N., Hill, J. E., Nousek, J. A., et al. 2005, SSRv, 120, 165
Cavecchi, Y., Patruno, A., Haskell, B., et al. 2011, ApJL, 740, L8
Chen, Y.-P., Zhang, S., Torres, D. F., et al. 2011, A&A, 534, A101
Churazov, E., Sunyaev, R., Revnivtsev, M., et al. 2007, A&A, 467, 529
Day, C. S. R., & Done, C. 1991, MNRAS, 253, 35P

Degenaar, N., Altamirano, D., & Wijnands, R. 2012, ATel, 4219

Degenaar, N., Jonker, P. G., Torres, M. A. P., et al. 2010, MNRAS, 404, 1591

Degenaar, N., Wijnands, R., & Kaur, R. 2011, MNRAS, 414, L104

Falanga, M., Chenevez, J., Cumming, A., et al. 2008, A&A, 484, 43

Fujimoto, M. Y., Hanawa, T., & Miyaji, S. 1981, ApJ, 247, 267

Galloway, D. K., Muno, M. P., Hartman, J. M., Psaltis, D., & Chakrabarty, D. 2008, ApJS, 179, 360

in 't Zand, J. J. M., Cumming, A., van der Sluys, M. V., Verbunt, F., & Pols, O. R. 2005, A&A, 441, 675

in 't Zand, J. J. M., Galloway, D. K., & Ballantyne, D. R. 2011, A&A, 525, A111

in 't Zand, J. J. M., Homan, J., Keek, L., & Palmer, D. M. 2012, A&A, 547, A47

in 't Zand, J. J. M., & Weinberg, N. N. 2010, A&A, 520, A81

Kallman, T., & Bautista, M. 2001, ApJS, 133, 221

Keek, L., Galloway, D. K., in 't Zand, J. J. M., & Heger, A. 2010, ApJ, 718, 292

Kuulkers, E., den Hartog, P. R., in 't Zand, J. J. M., et al. 2003, A&A, 399, 663

Kuulkers, E., in 't Zand, J. J. M., & Lasota, J.-P. 2009, A&A, 503, 889

Lewin, W. H. G., van Paradijs, J., & Taam, R. E. 1995, in X-ray Binaries, ed. W. H. G. Lewin, J. van Paradijs, & E. P. J. van den Heuvel (Cambridge: Cambridge Univ. Press), 175

Linares, M., Altamirano, D., Chakrabarty, D., Cumming, A., & Keek, L. 2012, ApJ, 748, 82

Miller, J. M., Raymond, J., Fabian, A., et al. 2006, Natur, 441, 953

Miller, J. M., Raymond, J., Reynolds, C. S., et al. 2008, ApJ, 680, 1359

Molkov, S., Revnivtsev, M., Lutovinov, A., & Sunyaev, R. 2005, A&A, 434, 1069

Peng, F., Brown, E. F., & Truran, J. W. 2007, ApJ, 654, 1022

Remillard, R. A., & Levine, A. M. 2008, ATel, 1853

Ricci, C., Beckmann, V., Carmona, A., & Weidenspointner, G. 2008, ATel, 1840

Romano, P., Campana, S., Chincarini, G., et al. 2006, A&A, 456, 917

Schatz, H., & Rehm, K. E. 2006, NuPhA, 777, 601

Strohmayer, T., & Bildsten, L. 2006, New Views of Thermonuclear Bursts, ed. M. Lewin W. H. G. & van der Klis (Cambridge: Cambridge Univ. Press), 113

Strohmayer, T. E., & Brown, E. F. 2002, ApJ, 566, 1045

van Paradijs, J., Dotani, T., Tanaka, Y., & Tsuru, T. 1990, PASJ, 42, 633

Wilms, J., Allen, A., & McCray, R. 2000, ApJ, 542, 914

Yu, W., Li, T. P., Zhang, W., & Zhang, S. N. 1999, ApJL, 512, L35